

# OIPR: Evaluation for Time-series Anomaly Detection Inspired by Operator Interest

Yuhan Jing, Jingyu Wang, *Senior Member, IEEE*, Lei Zhang, Haifeng Sun, Bo He, Zirui Zhuang, Chengsen Wang, Qi Qi, *Senior Member, IEEE*, and Jianxin Liao, *Senior Member, IEEE*

**Abstract**—With the growing adoption of time-series anomaly detection (TAD) technology, numerous studies have employed deep learning-based detectors for analyzing time-series data in the fields of Internet services, industrial systems, and sensors. The selection and optimization of anomaly detectors strongly rely on the availability of an effective performance evaluation method for TAD. Since anomalies in time-series data often manifest as a sequence of points, conventional metrics that solely consider the detection of individual point are inadequate. Existing evaluation methods for TAD typically employ point-based or event-based metrics to capture the temporal context. However, point-based metrics tend to overestimate detectors that excel only in detecting long anomalies, while event-based metrics are susceptible to being misled by fragmented detection results. To address these limitations, we propose *OIPR*<sup>1</sup>, a novel set of TAD evaluation metrics. It models the process of operators receiving detector alarms and handling faults, utilizing area under the operator interest curve to evaluate the performance of TAD algorithms. Furthermore, we build a special scenario dataset to compare the characteristics of different evaluation methods. Through experiments conducted on the special scenario dataset and five real-world datasets, we demonstrate the remarkable performance of *OIPR* in extreme and complex scenarios. It achieves a balance between point and event perspectives, overcoming their primary limitations and offering applicability to broader situations.

**Index Terms**—Time-series, Anomaly Detection, Evaluation, Precision and Recall

## I. INTRODUCTION

Time-series anomaly detection (TAD) [1]–[4] refers to the detection of a series of points with temporal continuity to identify time points or ranges that deviate from normal patterns. TAD holds significant importance in various fields, including fault detection and troubleshooting in industrial systems [5], [6], Internet services [7]–[10], sensors [11]–[14]. Detectors used for anomaly detection can be supervised or unsupervised, with their performance typically evaluated using manually annotated labels. Operators compare the outputs of the detector with the ground truth labels and calculate one or more metrics to evaluate the performance. In the context of binary classification, classical point-wise (*PW*) metrics such as precision, recall, receiver operating characteristic (ROC)

Yuhan Jing, Jingyu Wang, Haifeng Sun, Bo He, Zirui Zhuang, Chengsen Wang, Qi Qi and Jianxin Liao are with the State Key Laboratory of Networking and Switching Technology, Beijing University of Posts and Telecommunications, Beijing 100876, China (e-mail: {jingyh, wangjingyu, hfsun, hebo, zhuangzirui, qiqi8266, cswang, liaojx}@bupt.edu.cn).

Lei Zhang is with the China United Network Communications Co., Ltd., Beijing 100033, China (zhangl83@chinaunicom.cn).

<sup>1</sup>The implementation of the proposed metrics and the special scenario dataset are available at <https://github.com/weatherjyh/OIPR>.

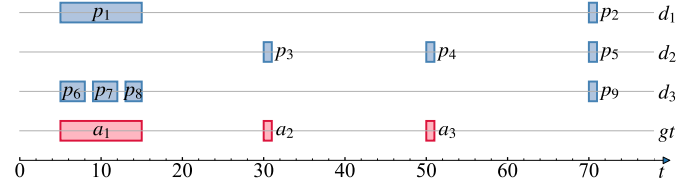


Fig. 1. An illustrative example highlighting the distinction between point-based and event-based methods, where  $d_1$ ,  $d_2$ , and  $d_3$  represent the results of three different anomaly detectors, and  $gt$  denotes the ground truth labels.

curve, and area under the ROC curve (AUROC) are commonly employed for the performance evaluation of general anomaly detection tasks [15], [16]. In the point-wise metrics, precision indicates the proportion of correctly identified positive points among all points predicted as positive, while recall represents the proportion of accurately predicted positive points relative to the total number of actual positive points.

However, due to the continuity of time-series data, large Internet companies commonly employ event-based metrics for data analysis. For instance, within MAXIMO<sup>2</sup>, the enterprise asset management system of IBM, the metrics of mean time to repair (MTTR) and mean time between failure (MTBF) are essential for assessing the availability and reliability of the system. They concentrate on capturing the frequency, duration, and recovery of each failure, signifying that ongoing events, rather than isolated time points, are regarded as the fundamental unit in maintenance operations. Therefore, researchers have recognized that the classical *PW* metrics are inadequate for TAD evaluation, as they treat each time point as an individual unit, failing to account for the temporal continuity of anomaly events. In recent years, improved TAD evaluation methods [17]–[20] that take the continuity of time-series into consideration have been proposed, which can be broadly classified into two categories: point-based and event-based methods. Point-based methods treat each anomaly point as equal, with specific predicted points adjusted to account for the temporal context. Meanwhile, event-based methods evaluate the detection performance based on anomaly events, irrespective of their durations. To illustrate the distinctions between the point-based and event-based methods, we present an example with three different detectors ( $d_1$ ,  $d_2$  and  $d_3$ ) applied to the same ground truth  $gt$  in Fig. 1.

We employ the point adjustment method (*PA*) [21] as a representative example of point-based methods. It accurately

<sup>2</sup><https://www.ibm.com/topics/mttr>

TABLE I  
THE EVALUATION RESULTS (P/R/F1) OF THE EXAMPLE IN FIG. 1 USING  
THE METHODS OF *PA* AND *TaPR*, RESPECTIVELY.

Methods	PA			TaPR		
	P	R	F1	P	R	F1
$d_1$	0.909	0.833	0.87	0.5	0.333	0.4
$d_2$	0.667	0.167	0.267	0.667	0.667	0.667
$d_3$	0.909	0.833	0.87	0.75	0.3	0.429

reflect the number of anomaly points, in line with the classical *PW* method. As a result, long anomaly events play a crucial role in the evaluation process of *PA*. As shown in Table I, the detector  $d_1$  identifies the longest anomaly event,  $a_1$ , leading to a high recall of 0.833. In contrast,  $d_2$  identifies two shorter anomaly events,  $a_2$  and  $a_3$ , resulting in a recall of only 0.167. *PA* assigns the detector that identifies more anomalies with a significantly lower f-score, which contradicts the intuitive expectations of the operators.

Differently, event-based evaluation methods, such as *TaPR* [22], treat each anomaly event as equal. For example, the recall of  $d_1$  is 0.333 (one event detected out of three) in the evaluation of *TaPR*, while for  $d_2$ , it is 0.667 (two events detected out of three). Therefore, *TaPR* appears to provide a more reasonable evaluation of  $d_1$  and  $d_2$  compared to *PA*. However, consider a scenario where two false positive (FP) points are inserted into  $d_1$  to create  $d_3$ , which simulates the noise interference that reduces detector performance. From an event-based perspective, the number of successfully detected events increases from 1 to 3, leading to a precision increase from 0.5 to 0.75 and an f1-score rise from 0.4 to 0.429. This issue arises from the fragmentation of predicted events, complicating the ranking of fragmented versus complete events in event-based evaluations. Thus, an exclusive focus on event equality can yield misleading conclusions.

To overcome the above limitations of point-based and event-based methods, we introduce a set of novel TAD performance evaluation metrics, named *OIPR* (*Operator Interest-based Precision and Recall* metrics). It models the evolving interest of operators during the troubleshooting process, achieves a balance between point-based and event-based perspectives and is suitable for a broader range of scenarios. Additionally, we provide an artificial dataset containing nine special scenarios to analyze the characteristics of different evaluation methods under diverse boundary conditions. Experiments on five real-world datasets are also conducted to investigate the efficacy of different evaluation methods in intricate practical scenarios.

The main contributions of this work are as follows:

- We propose a novel TAD evaluation method that models the dynamic changes in operator interest while monitoring the time-series data and responding to detector alarms in real-world scenarios. It addresses the challenges posed by long anomaly events and fragmented detection results, and innovatively calculates the precision and recall using the area under the operator interest curve.
- We establish a special scenario dataset that allows for a comprehensive analysis of characteristics of various TAD methods across diverse boundary conditions. This

dataset serves as a valuable research materials for future investigations of TAD evaluation.

- We conduct experiments on five real-world datasets using both representative and adversarial TAD algorithms. The results indicate that *OIPR* outperforms the baseline evaluation methods, exhibiting fewer limitations and greater applicability across a variety of real-world scenarios.

## II. RELATED WORK

### A. Time-series Anomaly Detection

Anomalies in time-series datasets can originate from a variety of sources, resulting in distinct anomaly characteristics. For instance, external attacks can lead to service interruptions, which are often reflected as abrupt fluctuations in the time-series data [23]. Additionally, hardware failures, such as hard drive malfunctions or network device outages, can result in a significant decline in system performance, causing a sustained deterioration of the associated indicators [24]. Furthermore, the deployment or changes of services can induce variations in the corresponding key performance indicators (KPIs) over time, potentially triggering a series of consecutive or intermittent anomaly points [25]. In terms of duration, anomalies can manifest at specific time points or persist across a sequence of consecutive time points [26]. The latter is referred to as an anomaly event that encompasses multiple anomaly points.

Typical techniques for TAD encompass a range of approaches, including statistical [27], machine learning [28], and deep learning [21], [29] algorithms. Time-series data is generally collected at regular intervals from various agents or sensors, with each time point representing a distinct sample. The detection results generated by the anomaly detector maintain the same discreteness and sampling frequency as the input data. After the process of detection, the discrete results can be systematically organized into predicted events based on temporal continuity, and compared with the ground truth labels to evaluate the performance of TAD. However, establishing a reliable mapping between the ground truth anomaly events and the detection results presents notable challenges. Specifically, temporal factors such as incorrect insertions, deletions, fragmentation, and merging [30] introduce significant ambiguities into the mapping relationships, thereby complicating the performance evaluation of TAD.

### B. Existing TAD Evaluation Methods

Classical *PW* metrics of precision/recall (P/R) have been employed in the evaluation of conventional TAD tasks [15], [16]. However, recent studies have underscored the significance of considering the temporal continuity inherent in time-series data, leading to the development of specialized evaluation methods. The *PA* method was initially introduced in [21], which operates under the premise that if at least one point within an anomaly event is detected, the entire anomaly event is deemed successfully identified. Building upon this, the method of *PA%K* was proposed in [18], which stipulates that a minimum proportion of points within a ground truth event must be detected for the event to be classified as successfully detected. After adjusting the detection results in accordance

with their respective principles, both methods calculated the P/R metrics in the same manner as the classical *PW* method.

Different from the above point-based methods, event-based methods treat each continuous anomaly interval (i.e. anomaly event) as a single unit. The *RP/RR* method [19] introduced factors of existence, size, position, and cardinality detection for anomaly events, allowing for customizable functions or parameters for each factor. Meanwhile, *TaPR* [22] addressed the challenge of ambiguous labeling by evaluating each ground truth event or predicted event through a combination of detection scores and portion scores. Both *RP/RR* and *TaPR* regarded each ground truth event as equally significant, irrespective of its duration. This principle is similarly applied to the predicted events. Subsequently, the metrics of precision and recall are averaged across the ground truth and predicted events. Another event-based method, referred to as affiliation metrics (AM) [26], provided an alternative perspective in which each ground truth event is considered equal, but the predicted results are assigned, measured in points, to the affiliation zone of the nearest ground truth event. The metrics of precision and recall metrics are then averaged across the ground truth events.

### C. Summary

Depending on the specific focuses and assumptions, the previously mentioned TAD evaluation methods can yield significantly different outcomes. In certain extreme scenarios characterized by long anomaly events or fragmented detection results, the point-based and event-based evaluation methods will probably generate misleading results, thereby constraining their applicability [31]. In this study, we propose a comprehensive TAD evaluation method based on the operator interest to aid operators in selecting more effective detectors for practical applications, and demonstrate its robust performance on the special scenario dataset and five real-world datasets.

## III. MOTIVATION

### A. Problem Formulation

The problem of TAD and its evaluation can be formally articulated as follows: Given a time-series spanning  $T$  time points, denoted as  $\mathbf{x} = \{x_0, x_1, \dots, x_{T-1}\}$ , the corresponding ground truth labels are represented as  $\mathbf{y} = \{y_0, y_1, \dots, y_{T-1}\}$ , where  $y_t \in \{0, 1\}$  denotes whether the time-series is anomalous (1) or not (0) at time point  $t$ . For a specific anomaly detector, the detection results are denoted as  $\hat{\mathbf{y}} = \{\hat{y}_0, \hat{y}_1, \dots, \hat{y}_{T-1}\}$ .

The classical *PW* method evaluates the performance of TAD by calculating three primary metrics: precision (P), recall (R), and f1-score (F1). These metrics are defined as follows:

$$\begin{aligned} P &= \frac{TP}{TP + FP}, R = \frac{TP}{TP + FN}, \\ F1 &= \frac{2 \cdot P \cdot R}{P + R}, \end{aligned} \quad (1)$$

where TP, FP, and FN represent the number of true positive, false positive, and false negative points, respectively. Other specialized evaluation methods for TAD typically adopt the P/R format, with different solutions for precision and recall metrics. Ultimately, the metric of f1-score is calculated using the same methodology as outlined in (1).

### B. Limitations of Existing Evaluation Methods

1) *Long Anomaly Effect*: As a distinctive binary classification task, TAD prompts researchers to develop specialized evaluation methods that take into account the temporal continuity of events. In this context, the existence detection of a greater number of anomaly events, rather than detecting more individual anomaly points, has become the primary consideration for operators. However, in point-based evaluation methods, the significance attributed to anomaly events is linearly correlated with the number of points they encompass. As a result, a limited number of long anomalies can overshadow the influence of a larger quantity of shorter anomalies in the final evaluation outcomes. To demonstrate the impact of the long anomaly effect, we employ two straightforward adversarial algorithms, one of which is designated as the first point detector, denoted as  $d_{fp}$ . It is specifically designed to identify only the initial point of each ground truth event. During periods without any ground truth anomalies, the output of  $d_{fp}$  consistently remains at 0. While the first point detector successfully identifies the existence of every anomaly event, it lacks the ability to discern the durations of these anomalies.

Another adversarial algorithm, referred to as the long anomaly detector  $d_l(L)$ , is designed to identify the ground truth events within a given time-series that have a duration of at least  $L$ . Specifically,  $d_l(L)$  correctly detects all points that fall within the long ground truth events, while producing an output of 0 for all other time points. Although the long anomaly detector is effective in identifying anomaly events with long durations, it fails to detect the other shorter events.

For demonstration purposes, we extract a slice from the SMD dataset [3], using both  $d_{fp}$  and  $d_l$  for anomaly detection, as illustrated in Fig. 2. Among them,  $d_{fp}$  accurately reports the occurrence of all thirteen anomaly events, which holds significant value for operators. In contrast,  $d_l$  detects only three of these anomaly events. If it is deployed for fault detection in a service, operators will miss the opportunity to recognize these short anomaly events. Within the point-based evaluation methods, *PW* and *PA%K* fail to reflect this risk. As demonstrated in Table II,  $d_l$  achieves a high f1-score of 0.848 using both methods, while  $d_{fp}$  attains a significantly low f1-score of 0.371. This discrepancy arises due to the fact that  $d_l$  detects a greater number of anomaly points compared to  $d_{fp}$ . In contrast, the method of *PA* exhibits a distinct behavior of overestimation. It adjusts the detection result of  $d_{fp}$  to an ideal detector (whose outputs perfectly match the ground truth), even though it does not actually detect the duration of any event comprising more than one point.

Event-based evaluation methods, such as *RP/RR*, *TaPR*, and *AM*, are not impacted by the long anomaly effect. Their evaluation results for the detectors primarily depend on the number of anomaly events they detect, and  $d_{fp}$  is evaluated to be much better than  $d_l$ , as demonstrated in Table II.

2) *Fragmentation Effect*: Although using an event-based method can avoid the impact of the long anomaly effect, we have observed another misleading phenomenon, called the fragmentation effect, which stems from the discrete nature of the detection results. In instances where a ground truth event

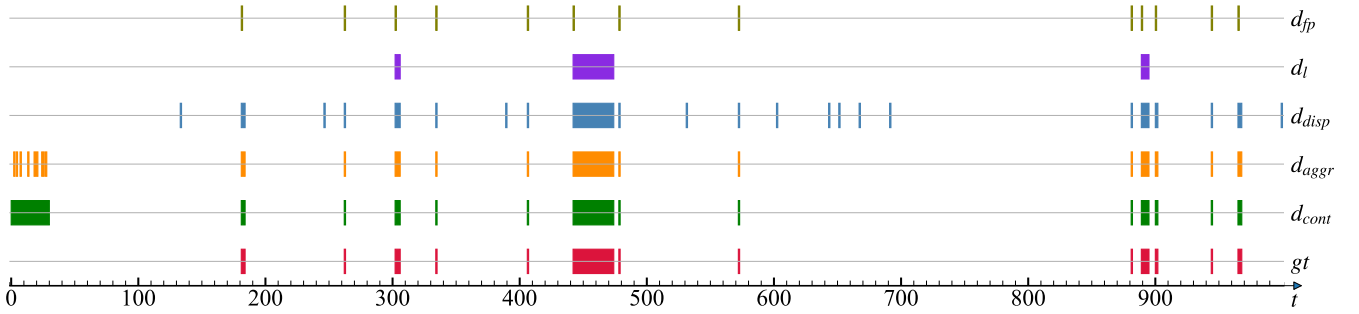


Fig. 2. A demonstration scenario which displays 5 adversarial algorithms, including the first point detector  $d_{fp}$ , the long anomaly detector  $d_l$ , the dispersed disturbance  $d_{disp}$ , the aggregated disturbance  $d_{agg}$ , and the continuous disturbance  $d_{cont}$ .

TABLE II  
THE F1-SCORES OF THE DEMONSTRATION IN FIG. 2 USING DIFFERENT EVALUATION METHODS. THE BOLD RESULTS ARE THE HIGHEST F1-SCORES IN THE CORRESPONDING GROUPS.

Adversarial Algorithms	PW	PA	PA%K	RP/RR	TaPR	AM	OIPR (Ours)
$d_{fp}$	0.371	<b>1.000</b>	0.371	<b>0.926</b>	<b>0.908</b>	<b>0.964</b>	<b>0.896</b>
$d_l, L = 4$	<b>0.848</b>	0.848	<b>0.848</b>	0.375	0.375	0.375	0.552
$d_{disp}$	<b>0.919</b>	<b>0.919</b>	<b>0.919</b>	0.722	0.722	0.942	0.761
$d_{agg}$	<b>0.919</b>	<b>0.919</b>	<b>0.919</b>	0.788	0.788	<b>0.972</b>	<b>0.912</b>
$d_{agg}$	0.792	0.792	0.792	<b>0.962</b>	<b>0.962</b>	0.966	0.903

comprises a series of points, the detector is likely to identify only a subset of points that exhibit significant deviations from the normal pattern [18]. Consequently, a contiguous event can be fragmented into multiple events in the detection results. The fragmentation effect leads to an increase in the number of true positive events, despite the fact that the successful detection is confined to a single original contiguous event. This phenomenon can also arise when the detector experiences a short-term, one-time disturbance, such as during a service deployment or change. In such cases, the detector is prone to generating a high frequency of false positive points, leading to multiple fragmented false positive events that originate from the same underlying cause. To empirically illustrate the fragmentation effect, we introduce three specific disturbances to the ideal detector, as depicted in Fig. 2:

**Dispersed disturbance  $d_{disp}$ :** To simulate the interference induced by random noise, we generate a set of FP points, constituting 1% of the entire time-series, which are then randomly inserted throughout the detection results.

**Aggregated disturbance  $d_{agg}$ :** To simulate the short-term, intermittent disturbances associated with the deployment or change of the service, we randomly introduce a set of FP points, comprising 1% of the entire time-series, into the initial 3% of the detection results.

**Continuous disturbance  $d_{cont}$ :** The initial 3% of the detection results is configured to a value of 1 to simulate a short-term, continuous disturbance scenario resulting from the deployment or change of the service.

In the above three cases, both  $d_{agg}$  and  $d_{cont}$  necessitate operators to monitor the system status for a period following

initialization. During the subsequent long-term operation, the detector exhibits a high level of reliability. In contrast,  $d_{disp}$  poses a significant challenge for operators due to its persistent and recurrent generation of false alarms, which ultimately results in resource wastage. As a result,  $d_{disp}$  leads to a more significant decline in the practical utility of the detector.

As illustrated in Table II, the point-based methods, namely  $PW$ ,  $PA$ , and  $PA\%K$ , consider  $d_{cont}$  as the worst-performing detector due to its highest number of false positive points, without taking into account that these points originate from the same anomaly event. In contrast, the event-based methods,  $RP/RR$  and  $TaPR$ , suggest that both  $d_{agg}$  and  $d_{disp}$  exhibit similar poor performance, even though all false positive points in  $d_{agg}$  are concentrated within a limited period following initialization. Another method that is partially event-based,  $AM$ , remains unaffected by the fragmentation effect due to its exclusive adoption of an event-based perspective for the ground truth, rather than for the detection results.

### C. Towards A Universal TAD Evaluation Method

By means of the adversarial algorithms and demonstration outlined in the last section, we have elucidated the limitations of point-based and event-based evaluation methods. In pursuit of developing a more universally applicable TAD evaluation method, we have established two primary objectives:

**Existence detection reward.** The fundamental disparity between TAD and conventional binary classification tasks lies in the continuity of events. A universally applicable TAD evaluation method should possess the capability to reward the existence detection of the ground truth events. In this regard, the first point to detect the existence of an anomaly event should receive a higher reward than in classical  $PW$  metrics.

**Fragments Merging.** Given that time points serve as the fundamental units for the collection of time-series data, the detection results inherently exhibit a discrete nature. Therefore, a universal TAD evaluation method should take into account the potential merging of fragmented events and effectively differentiate between dispersed and aggregated anomaly points.

In addition to the above two objectives, it is also advisable for evaluation methods to incorporate several other beneficial characteristics, such as addressing ambiguous labeling [22] and providing early detection reward [19]. Further exploration

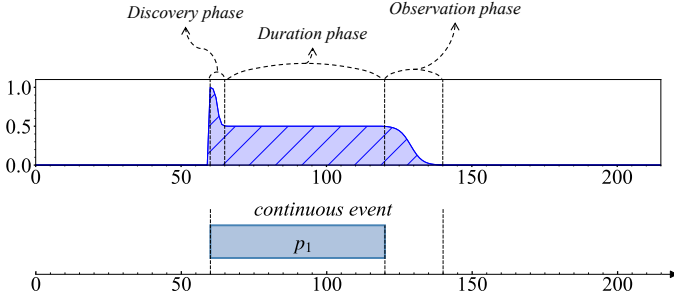


Fig. 3. An example of the operator interest curve for an individual continuous anomaly event.

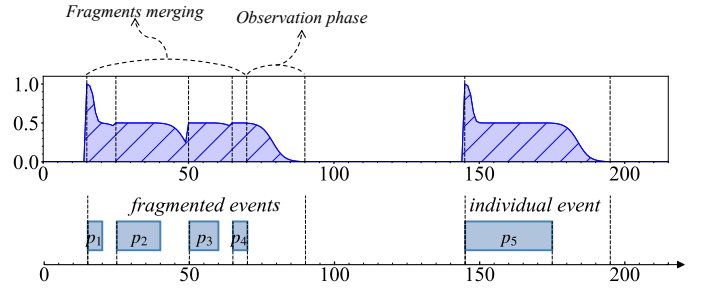


Fig. 4. An example of the operator interest curve for fragmented anomaly events.

of evaluator characteristics will be discussed in the context of special scenario dataset experiments in Section IV.

To develop a more universally applicable evaluation method for TAD that aligns closely with the work habits of operators, we drew inspiration from the real-world behaviors of operators monitoring anomaly detection alarms. (i) Typically, operators deploy anomaly detectors for specific KPIs and check the system status upon receiving anomaly alarms to ascertain the presence of any faults. We define the stage during which a detector reports an anomaly point, thereby prompting the operator to closely monitor the relevant KPIs and initiate system status checks, as the “discovery phase” of a suspected fault. (ii) Subsequently, actions are implemented to address the fault, while the detector continuously or intermittently reports anomaly points. At this stage, operators maintain a level of interest in the event, referred to as the “duration phase”. (iii) Finally, after implementing several repairs, the problem was solved and the detector ceased reporting anomalies. Operators will continue to monitor this fault during what we refer to as the “observation phase” to ensure its recovery. Motivated by the aforementioned observations, we propose a universal TAD evaluation method that utilizes the operator interest curve to calculate performance metrics. This method offers an existence detection reward for the first detected point in each event and enables the merging of potentially fragmented events.

#### IV. PROPOSED METHOD

##### A. Operator Interest Curve

In this section, we outline the methodology employed to derive the operator interest curve for anomaly detection, which captures the dynamics of operators in discovering and handling the anomalies. To construct the operator interest curve, we propose a set of functions, denoted as  $\Phi(i)$ , which characterize the phases of discovery, duration, and observation associated with an individual anomaly event:

$$\Phi(i) = \begin{cases} \omega(i), & 0 \leq i < l_{dis} + l_{dur} \\ \omega(l_{dis} + l_{dur}) \times \gamma(i - l_{dis} - l_{dur} + 1), & l_{dis} + l_{dur} \leq i < l_{dis} + l_{dur} + l_{obs} \\ 0, & i \geq l_{dis} + l_{dur} + l_{obs} \end{cases}, \quad (2)$$

where  $i$  represents the distance from the current point to the initial point of the anomaly event. The discovery and duration

phases of the anomaly event are characterized by a shared continuous interest function  $\omega(\cdot)$ , while  $\gamma(\cdot)$  represents the operator interest for the observation phase. The pre-configured integer parameters for the lengths of the discovery phase and observation phase are denoted as  $l_{dis}$  and  $l_{obs}$ , respectively. The length of the duration phase,  $l_{dur}$ , can be calculated by subtracting  $l_{dis}$  from the total length of the anomaly event.

Fig. 3 presents an example of the operator interest curve for an individual continuous event. As a default approach, we employ a reversed and scaled sigmoid function for  $\omega(\cdot)$ :

$$\omega(i) = \begin{cases} 1, & i = 0 \\ b_{dur} + (1 - b_{dur}) \times \frac{1 - \text{sigmoid}(\frac{10}{l_{dis}}i - 5)}{1 - \text{sigmoid}(-5)}, & i > 0 \end{cases}, \quad (3)$$

where  $\text{sigmoid}(x) = \frac{1}{1 + e^{-x}}$ , and  $b_{dur}$  denotes the lower boundary of operator interest for the discovery and duration phases. Initially, the operator interest is set to 1 upon the detection of an anomaly event, then progressively diminishes throughout the discovery phase and ultimately approaching a level near  $b_{dur}$ . In the subsequent duration phase, the operator interest continues to decline but remains above  $b_{dur}$ . The rate of decrease is determined by the configuration of  $l_{dis}$ , which is set by default to 1/4 of the average length of the ground truth events, rounded up to the nearest integer.

The interest function for the observation phase,  $\gamma(i)$ , is calculated according to (4):

$$\gamma(i) = \begin{cases} 1, & i = 0 \\ \frac{1 - \text{sigmoid}(\frac{10}{l_{obs}}i - 5)}{1 - \text{sigmoid}(-5)}, & 0 < i \leq l_{obs} \\ 0, & i > l_{obs} \end{cases}. \quad (4)$$

The operator interest decreases from its value at the end of the duration phase to 0 during the observation phase, as shown in Fig. 3. The rate of decline is determined by the parameter  $l_{obs}$ , where a shorter  $l_{obs}$  leads to a more rapid reduction in operator interest. Typically, the default value of  $l_{obs}$  is set to the average length of the ground truth events.

##### B. Merging Fragmented Anomaly Events

In the previous section, we introduced the operator interest curve for an individual continuous anomaly event. However, it is essential to recognize that the anomaly events in the

detection results can be fragmented. To address this issue, we propose a forward process for the online calculation of the operator interest curve, which is detailed in Algorithm 1.

---

**Algorithm 1:** Online calculation process of the operator interest curve for the detection results

---

**Input:** the detection results  $\hat{y} = \{\hat{y}_0, \hat{y}_1, \dots, \hat{y}_{T-1}\}$ , and the pre-configured parameters  $l_{dis}$ ,  $l_{obs}$  and  $b_{dur}$ .

**Output:** the operator interest  $\hat{I}$  for the detection results  $\hat{y}$ .  
( $T+l_{obs}$ ) zeros

```

1:  $\hat{I} \leftarrow \{0, 0, \dots, 0\}$ 
2:  $p_{start} \leftarrow -l_{obs} - 1$ 
3:  $p_{end} \leftarrow -l_{obs} - 1$ 
4:  $t \leftarrow 0$ 
5: while  $t < T$  do
6:   if  $\hat{y}_t = 1$  then
7:     if  $t - p_{end} > l_{obs}$  then
8:        $p_{start} \leftarrow t$ 
9:     end if
10:     $\hat{I}_t \leftarrow \omega(t - p_{start})$ 
11:     $p_{end} \leftarrow t$ 
12:  else
13:    if  $t - p_{end} \leq l_{obs}$  then
14:       $\hat{I}_t \leftarrow \omega(t - p_{start}) \cdot \gamma(t - p_{end})$ 
15:    end if
16:  end if
17:   $t \leftarrow t + 1$ 
18: end while
19: while  $t < T + l_{obs}$  do
20:   if  $t - p_{end} \leq l_{obs}$  then
21:     $\hat{I}_t \leftarrow \omega(t - p_{start}) \cdot \gamma(t - p_{end})$ 
22:   end if
23:    $t \leftarrow t + 1$ 
24: end while
25:  $\hat{I} \leftarrow \{\hat{I}_0, \hat{I}_1, \dots, \hat{I}_{T-1+l_{obs}}\}$ 
26: return  $\hat{I}$ 

```

---

Fig. 4 presents an example of the operator interest curve for fragmented anomaly events. Temporary interruptions in reporting anomaly points result in a decline in the operator interest, though it does not drop to 0 immediately. If new anomaly points are reported within  $l_{obs}$ , the fragmented anomaly events are merged. Conversely, if a new anomaly point is reported after the end of the last observation phase, it is classified as the initiation of a distinct individual anomaly event.

By employing the same methodology as outlined in Algorithm 1, we can derive the operator interest curve of the ground truth labels, denoted as  $I$ . While the ground truth are not impacted by the fragmentation effect, its operator interest curve represents the anticipated troubleshooting process of the ideal detector and serves as a benchmark for evaluation.

### C. Precision and Recall Metrics in OIPR

The evaluation metrics of precision and recall in OIPR are derived using the operator interest curves. In this work, conventional number of true positive points is replaced with the true positive area  $TP_{oi}$ , which measures the overlapping

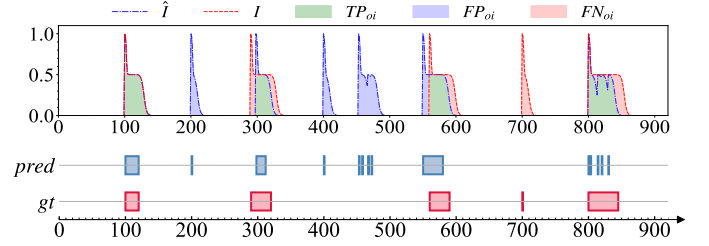


Fig. 5. Visualization of the overlapping area of operator curves, corresponding to  $TP_{oi}$ ,  $FP_{oi}$ , and  $FN_{oi}$ .

area between the operator interest curve of the ground truth,  $I$ , and that of the detection results,  $\hat{I}$ . Likewise, the number of predicted positive points is represented as the area under  $\hat{I}$ . Therefore, the values for true positive area  $TP_{oi}$  and false positive area  $FP_{oi}$  in OIPR are defined as:

$$TP_{oi} = \text{AUC}(\min(I, \hat{I})), \quad (5)$$

$$FP_{oi} = \text{AUC}(\hat{I}) - TP_{oi}, \quad (6)$$

where  $\text{AUC}(\cdot)$  refers to the computation of the area under a specific curve, while  $\min(\cdot)$  indicates the selection of the smaller value between two time-series at each time point to generate a new sequence. Subsequently, the precision metric in OIPR, denoted as  $P_{oi}$ , is defined as:

$$P_{oi} = \frac{TP_{oi}}{TP_{oi} + FP_{oi}} = \frac{\text{AUC}(\min(I, \hat{I}))}{\text{AUC}(\hat{I})}. \quad (7)$$

Using a similar methodology, we transform the positive points in the ground truth to the area under the the operator interest curve for ground truth,  $I$ , and the false negative area  $FN_{oi}$  are calculated as follows:

$$FN_{oi} = \text{AUC}(I) - TP_{oi}. \quad (8)$$

The recall metric in OIPR, denoted as  $R_{oi}$ , is defined as:

$$R_{oi} = \frac{TP_{oi}}{TP_{oi} + FN_{oi}} = \frac{\text{AUC}(\min(I, \hat{I}))}{\text{AUC}(I)}. \quad (9)$$

Fig. 5 presents a visual illustration of  $TP_{oi}$ ,  $FP_{oi}$ , and  $FN_{oi}$ . Using the specialized precision and recall metrics in OIPR, the corresponding f1-score can be derived in a manner consistent with the classical method outlined in (1).

## V. EXPERIMENTS

### A. Experimental Setup

**Baseline TAD evaluation methods.** To evaluate the proposed OIPR method, we conducted a comparative analysis against six baseline methods in the context of TAD evaluation. The baseline methods include three point-based methods: the classical point-wise method *PW*, the point adjustment method *PA* [21], and the top-k point adjustment method *PA%K* [18]. In addition, three event-based methods are also included: the range-based TAD metrics *RP/RR* [19], the time-series aware metrics *TaPR* [22], and the affiliation metrics *AM* [26].

TABLE III  
PARAMETERS EMPLOYED IN THE EXPERIMENTS.  $\bar{L}_a$  MEANS THE  
AVERAGE LENGTH OF THE GROUND TRUTH EVENTS WITHIN THE DATASET.

Method	Parameter	Value
<b>PA%K</b>	Percentage threshold $K$	50
	Relative weight of existence reward $\alpha$	0.5
<b>RP/RR</b>	Overlap cardinality function $\gamma(\cdot)$	$1/x$
	Positional bias function $\delta(\cdot)$	front-end bias for RR, flat bias for RP
	Overlap size function $\omega(\cdot)$	default function in [19]
<b>TaPR</b>	Relative weight of detection score $\alpha$	0.5
	Number of Ambiguous Points $\delta$	5 for SMD/Special Scenarios, $\bar{L}_a$ for other datasets
	Detection possibilities threshold $\theta$	0
<b>OIPR (Ours)</b>	Length of discovery phase $l_{dis}$	5 for SMD/Special Scenarios, $\bar{L}_a/4$ for other datasets
	Length of observation phase $l_{obs}$	20 for SMD/Special Scenarios, $\bar{L}_a$ for other datasets
	Lower bound of interest in duration phase $b_{dur}$	0.5

The parameters employed for the baseline methods and our proposed method are summarized in Table III.

**Datasets.** The experiments are conducted on a special scenario dataset and five real-world datasets.

- **Special scenario dataset.** We have constructed an artificial dataset consisting of 24 evaluator-sensitive cases specifically designed for the evaluation of TAD. These cases are categorized into 9 distinct scenarios, each crafted to emphasize up to two evaluator characteristics. By leveraging the special scenario dataset, we can effectively demonstrate the limitations of various evaluation methods in a clear and concise manner.
- **Real-world datasets.** We have selected five time-series datasets for the experiments, namely MSL [32], SMAP [32], PSM [33], SMD [3], and SWaT [34]. To obtain the anomaly detection results on these datasets, we employ three advanced TAD models: Autoformer [35], DLinear [36], and Timesnet [37]. Furthermore, the five adversary algorithms proposed in Section III are also utilized.

## B. Experimental Results

### 1) Experimental Results on the Special Scenario Dataset:

In this section, we present several significant qualitative conclusions derived from the experiments conducted on the special scenario dataset, as illustrated in Table IV. The beneficial characteristics are emphasized in bold. The presence of beneficial characteristics in the evaluator is indicated with a checkmark ( $\checkmark$ ), while their absence is represented by a cross ( $\times$ ). Misleading characteristics are underlined, with a circle ( $\circ$ ) indicating the presence of such characteristics in the evaluator, while a dash (-) denotes their absence. A comprehensive introduction and detailed experimental results pertaining to the special scenario dataset are presented in the Appendix. Apart

from the characteristics of existence detection reward and fragments merging mentioned in Section III-C, we introduce seven additional evaluator characteristics in this section:

- **Overlapping proportion awareness:** For a specific ground truth event, a detector that identifies a greater proportion of anomaly points within it should be awarded a higher recall reward. This characteristic encourages the detector to identify as many points as possible within a single ground truth event, thereby improving the accuracy of event duration reporting.
- **Fragmented results penalty:** If a detector identifies a single ground truth event using an excessive number of fragmented events, its recall score should be penalized. This characteristic encourages the detector to achieve the identification of a single event using fewer fragments.
- **Addressing ambiguous labels:** The manual labeling process introduces ambiguity in defining anomaly event boundaries, resulting in anomalies affecting points before or after the ground truth event. Detecting these ambiguous points indicates a partial success in identifying the anomaly. Consequently, evaluation methods that address ambiguous labels should reward recall for these points.
- **Early detection reward:** It encourages detectors to identify anomalies early in the occurrence of the ground truth events, thereby improving the detection timeliness.
- **Fragmentation misleading in precision:** This misleading characteristic is present in several event-based evaluation methods. Detectors identifying a ground truth event through multiple fragmented events can achieve higher precision scores than those detect using a complete event. This discrepancy primarily arises from the misleading increase in the count of true positive events.
- **Long anomaly misleading:** This misleading characteristic is present in most point-based evaluation methods, where the significance of long anomalies far surpasses that of short anomalies. Consequently, detectors that identify more short anomalies may be outperformed by those that focus solely on long anomalies, hindering the detection of a more diverse range of anomalies.
- **Sparse anomaly misleading:** A pitfall observed in the *AM* method. The f1-score is overestimated due to the mapping from long absolute distance to limited relative precision and recall distances.

Among the above characteristics, *OIPR* effectively incorporates all beneficial factors while minimizing potential misleading influences. Compared to the baseline point-based and event-based methods, it offers enhanced universality and reduces deficiencies in extreme scenarios.

2) *Experimental Results on Real-World Datasets:* For real-world datasets, we categorize all experiments into three groups. The first group comprises the advanced TAD models Autoformer, DLinear, and Timesnet. The second group consists of the adversarial algorithms  $d_{fp}$  and  $d_l$ . The third group includes the adversarial algorithms  $d_{disp}$ ,  $d_{aggr}$ , and  $d_{cont}$ . The results of the three groups are summarized in Table V.

In the first group of experiments, different evaluation methods lead to varying rankings of the TAD models. Point-based methods, namely *PW*, *PA*, and *PA%K*, assign the highest

TABLE IV  
QUALITATIVE CONCLUSIONS DERIVED FROM EXPERIMENTS ON THE SPECIAL SCENARIO DATASET.

Evaluator Characteristics	PW	PA	PA%K	RP/RR	TaPR	AM	OIPR(Ours)
Existence detection reward	×	✓	*Piecewise	✓	✓	✓	✓
Overlapping proportion awareness	✓	×	*Piecewise	✓	✓	✓	✓
Fragmented results penalty	×	×	×	✓	×	×	✓
Fragments Merging	×	×	×	×	×	×	✓
Addressing ambiguous labels	×	×	×	×	*Only delay	✓	✓
Early detection reward	×	×	×	✓	×	×	✓
Fragmentation misleading in precision	-	-	-	○	○	-	-
Long anomaly misleading	○	○	○	-	-	-	*Mitigated
Sparse anomaly misleading	-	-	-	-	-	○	-
Number of custom parameters (functions)	0	0	1	4	4	0	3

\*Piecewise: According to the custom configuration of parameter  $K$ , the  $PA\%K$  method has overlapping proportion awareness only in the  $\leq K$  percentage segment of events, and the existence detection reward only in the  $> K$  percentage segment.

\*Only delay: The ambiguous points after the end of the events are considered, while those before the start of the event are not.

\*Mitigated: The influence of long anomaly misleading is mitigated rather than eliminated.

f1-scores to Timesnet on MSL and SMAP datasets, while the event-based methods  $RP/RR$  and  $TaPR$  deem DLinear to perform the best. This discrepancy is largely due to Timesnet generating a higher number of both TP and FP points compared to DLinear. Point-based methods do not attach much importance to dispersed FP points due to their relatively small quantity compared to TP points. However, in event-based methods, the number of FP events formed by these dispersed FP points becomes significant in relation to the number of TP events, rendering them difficult to dismiss. Similarly, for  $OIPR$ , the observation phases generated by dispersed FP points impose a considerable penalty on precision. Consequently, DLinear is considered as the optimal detector for the MSL and SMAP datasets in  $RP/RR$ ,  $TaPR$ , and  $OIPR$ . For the  $AM$  method, the employment of affiliation zones and relative distances results in a more favorable evaluation of detectors that yield a larger number of predicted positive points, such as Autoformer for MSL and Timesnet for SMAP.

The second group of experiments is conducted to compare the impact of the long anomaly effect on different evaluation methods. Both  $PW$  and  $PA\%K$  methods are significantly impacted, as they favor  $d_l$  over  $d_{fp}$  across all datasets. Due to an overestimation of the performance in long anomaly detection,  $PA$  mistakenly considers that  $d_{fp}$  represents an ideal case, resulting in an f1-score of 1. In contrast, the event-based methods,  $RP/RR$ ,  $TaPR$ , and  $AM$ , remain unaffected by the long anomaly effect. For each dataset, the event-based methods consistently yield higher f1-scores for  $d_{fp}$  in comparison to  $d_l$ . As for  $OIPR$ , it mitigates the impact of the long anomaly effect rather than totally eliminating it. This is evidenced by its assigned f1-score to  $d_l$ , which is higher than that of the event-based methods and lower than that of the point-based methods. The fundamental principle underlying  $OIPR$  is that when the durations of all anomaly events are relatively short, the total number of events becomes a critical factor, suggesting that detectors capable of identifying all anomalies are suffice. In contrast, in instances where anomalies persist for significantly prolonged durations—such as the case of the longest anomaly

event lasting nearly 10 hours in the SWaT dataset, compared to the shortest anomaly event, which lasts only approximately 100 seconds—it is more rational to assign greater significance to the former. This approach is preferable to treating both events as entirely equivalent. Consequently,  $OIPR$  establishes a non-linear mapping between the durations of the ground truth events and their contributions to the evaluation outcomes, indicating that the impact of long anomalies is reduced in comparison to that observed in point-based methods.

The third group of experiments aims to assess the impact of the fragmentation effect. For this purpose, we introduce a measure referred to as the ratio of normal intervals containing false positive points, denoted as  $R_N$ . It quantifies the proportion of normal intervals that are contaminated by FP points, relative to the total number of normal intervals. In this context, normal intervals are defined as the non-anomalous intervals between two adjacent anomaly events in the ground truth. A higher value of  $R_N$  correlates with an increased likelihood that operators will encounter disturbances caused by false alarms during their daily activities. Table VI presents the  $R_N$  values corresponding to the detection results of three adversarial algorithms,  $d_{disp}$ ,  $d_{aggr}$ , and  $d_{cont}$ , across all datasets. It is evident that  $d_{disp}$  introduces a significant number of contaminated normal intervals, which consequently leads to a high value of  $R_N$ . In contrast, both  $d_{aggr}$  and  $d_{cont}$  yield small  $R_N$  values, indicating a low number of contaminated normal intervals. All three point-based methods and  $AM$  suggest that the performance of the detector  $d_{disp}$  is satisfactory due to its low count of FP points, despite the fact that it generates a substantial number of dispersed FP events. Differently, both  $RP/RR$  and  $TaPR$  contend that  $d_{disp}$  performs inadequately. However, they also suggest that  $d_{aggr}$  exhibits poor performance, despite its very low  $R_N$ . Notably, only  $OIPR$  assigns significantly higher f1-scores to  $d_{aggr}$  and  $d_{cont}$  compared to  $d_{disp}$ , as it takes into account the actual distribution of the discrete FP points.

Additional statistics for the real-world datasets are presented in Table VI, where  $N$  denotes the number of sample points within each dataset.  $\bar{L}_a$  represents the average length of



TABLE V  
EXPERIMENTAL RESULTS OF REAL-WORLD DATASETS. THE BOLD SCORES REPRESENT THE RESULT WITH THE HIGHEST F1-SCORE IN EACH GROUP.

Evaluation Method	Detector	MSL			SMAP			PSM			SMD			SWaT		
		P	R	F1	P	R	F1	P	R	F1	P	R	F1	P	R	F1
PW	Autoformer	0.81	0.721	0.763	0.541	0.614	0.575	1.0	0.789	0.882	0.77	0.659	0.71	1.0	0.656	0.792
	DLinear	0.963	0.604	0.742	0.983	0.524	0.684	0.998	0.932	<b>0.964</b>	0.901	0.819	<b>0.858</b>	1.0	0.926	<b>0.961</b>
	Timesnet	0.88	0.723	<b>0.794</b>	0.807	0.605	<b>0.692</b>	0.932	0.95	0.941	0.855	0.826	0.84	0.747	0.931	0.829
	$d_{fp}$	1.0	0.005	0.009	1.0	0.001	0.002	1.0	0.003	0.006	1.0	0.395	0.566	1.0	0.001	0.001
	$d_l$	1.0	0.529	<b>0.692</b>	1.0	0.455	<b>0.625</b>	1.0	0.365	<b>0.535</b>	1.0	0.572	<b>0.728</b>	1.0	0.657	<b>0.793</b>
	$d_{disp}$	0.913	1.0	<b>0.955</b>	0.928	1.0	<b>0.962</b>	0.965	1.0	<b>0.982</b>	0.81	1.0	<b>0.895</b>	0.924	1.0	<b>0.96</b>
	$d_{aggr}$	0.913	1.0	<b>0.955</b>	0.928	1.0	<b>0.962</b>	0.965	1.0	<b>0.982</b>	0.81	1.0	<b>0.895</b>	0.924	1.0	<b>0.96</b>
	$d_{cont}$	0.704	1.0	0.826	0.723	1.0	0.839	0.853	1.0	0.921	0.459	1.0	0.629	0.752	1.0	0.858
PA	Autoformer	0.842	0.902	0.871	0.6	0.781	0.678	1.0	0.822	0.902	0.77	0.659	0.71	1.0	0.657	0.793
	DLinear	0.968	0.71	0.819	0.984	0.57	0.722	0.998	0.981	<b>0.99</b>	0.901	0.819	<b>0.858</b>	1.0	0.958	<b>0.979</b>
	Timesnet	0.897	0.854	<b>0.875</b>	0.844	0.783	<b>0.812</b>	0.935	0.999	0.966	0.855	0.826	0.84	0.752	0.958	0.843
	$d_{fp}$	1.0	1.0	<b>1.0</b>	1.0	1.0	<b>1.0</b>	1.0	1.0	<b>1.0</b>	1.0	1.0	<b>1.0</b>	1.0	1.0	<b>1.0</b>
	$d_l$	1.0	0.529	0.692	1.0	0.455	0.625	1.0	0.365	0.535	1.0	0.572	0.728	1.0	0.657	0.793
	$d_{disp}$	0.913	1.0	<b>0.955</b>	0.928	1.0	<b>0.962</b>	0.965	1.0	<b>0.982</b>	0.81	1.0	<b>0.895</b>	0.924	1.0	<b>0.96</b>
	$d_{aggr}$	0.913	1.0	<b>0.955</b>	0.928	1.0	<b>0.962</b>	0.965	1.0	<b>0.982</b>	0.81	1.0	<b>0.895</b>	0.924	1.0	<b>0.96</b>
	$d_{cont}$	0.704	1.0	0.826	0.723	1.0	0.839	0.853	1.0	0.921	0.459	1.0	0.629	0.752	1.0	0.858
PA%K	Autoformer	0.831	0.835	0.833	0.556	0.653	0.6	1.0	0.81	0.895	0.77	0.659	0.71	1.0	0.657	0.793
	DLinear	0.968	0.701	0.813	0.984	0.56	0.714	0.998	0.973	<b>0.986</b>	0.901	0.819	<b>0.858</b>	1.0	0.958	<b>0.979</b>
	Timesnet	0.895	0.835	<b>0.864</b>	0.816	0.642	<b>0.719</b>	0.935	0.995	0.964	0.855	0.826	0.84	0.752	0.958	0.843
	$d_{fp}$	1.0	0.005	0.009	1.0	0.001	0.002	1.0	0.128	0.226	1.0	0.395	0.566	1.0	0.001	0.001
	$d_l$	1.0	0.529	<b>0.692</b>	1.0	0.455	<b>0.625</b>	1.0	0.365	<b>0.535</b>	1.0	0.572	<b>0.728</b>	1.0	0.657	<b>0.793</b>
	$d_{disp}$	0.913	1.0	<b>0.955</b>	0.928	1.0	<b>0.962</b>	0.965	1.0	<b>0.982</b>	0.81	1.0	<b>0.895</b>	0.924	1.0	<b>0.96</b>
	$d_{aggr}$	0.913	1.0	<b>0.955</b>	0.928	1.0	<b>0.962</b>	0.965	1.0	<b>0.982</b>	0.81	1.0	<b>0.895</b>	0.924	1.0	<b>0.96</b>
	$d_{cont}$	0.704	1.0	0.826	0.723	1.0	0.839	0.853	1.0	0.921	0.459	1.0	0.629	0.752	1.0	0.858
RP/RR	Autoformer	0.041	0.608	0.077	0.01	0.483	0.02	0.833	0.395	0.536	0.818	0.534	0.646	0.75	0.019	0.037
	DLinear	0.128	0.423	<b>0.196</b>	0.179	0.456	<b>0.257</b>	0.653	0.685	<b>0.668</b>	0.765	0.737	<b>0.751</b>	1.0	0.806	<b>0.893</b>
	Timesnet	0.05	0.597	0.093	0.019	0.618	0.037	0.107	0.787	0.188	0.691	0.754	0.721	0.02	0.679	0.039
	$d_{fp}$	1.0	0.514	<b>0.679</b>	1.0	0.509	<b>0.675</b>	1.0	0.697	<b>0.821</b>	1.0	0.887	<b>0.94</b>	1.0	0.503	<b>0.669</b>
	$d_l$	1.0	0.139	0.244	1.0	0.104	0.189	1.0	0.014	0.027	1.0	0.203	0.338	1.0	0.029	0.056
	$d_{disp}$	0.047	1.0	0.091	0.016	1.0	0.031	0.077	1.0	0.143	0.632	1.0	0.774	0.008	1.0	0.016
	$d_{aggr}$	0.06	1.0	0.114	0.019	1.0	0.038	0.094	1.0	0.171	0.674	1.0	0.805	0.01	1.0	0.02
	$d_{cont}$	0.972	1.0	<b>0.986</b>	0.985	1.0	<b>0.992</b>	0.985	1.0	<b>0.993</b>	0.992	1.0	<b>0.996</b>	0.965	1.0	<b>0.982</b>
TaPR	Autoformer	0.144	0.739	0.241	0.097	0.617	0.167	0.889	0.399	0.551	0.818	0.542	0.652	0.999	0.029	0.056
	DLinear	0.197	0.449	<b>0.274</b>	0.286	0.529	<b>0.371</b>	0.77	0.719	<b>0.744</b>	0.774	0.752	<b>0.763</b>	1.0	0.828	<b>0.906</b>
	Timesnet	0.148	0.7	0.244	0.118	0.695	0.202	0.288	0.915	0.438	0.722	0.769	0.745	0.096	0.887	0.173
	$d_{fp}$	1.0	0.507	<b>0.673</b>	1.0	0.505	<b>0.671</b>	1.0	0.667	<b>0.801</b>	1.0	0.857	<b>0.923</b>	1.001	0.501	<b>0.668</b>
	$d_l$	1.0	0.139	0.244	1.0	0.104	0.189	1.0	0.014	0.027	1.0	0.212	0.35	1.0	0.029	0.056
	$d_{disp}$	0.133	1.0	0.234	0.119	1.0	0.213	0.237	1.0	0.383	0.641	1.0	0.781	0.083	1.0	0.154
	$d_{aggr}$	0.211	1.0	0.349	0.079	1.0	0.146	0.365	1.0	0.535	0.674	1.0	0.805	0.352	1.0	0.521
	$d_{cont}$	0.988	1.0	<b>0.994</b>	0.993	1.0	<b>0.996</b>	0.995	1.0	<b>0.997</b>	0.996	1.0	<b>0.998</b>	0.989	1.0	<b>0.994</b>
AM	Autoformer	0.756	0.956	<b>0.845</b>	0.513	0.731	0.603	0.965	0.43	0.595	0.941	0.543	0.689	1.0	0.029	0.056
	DLinear	0.736	0.626	0.677	0.739	0.661	0.698	0.938	0.796	0.861	0.955	0.749	0.84	1.0	0.825	<b>0.904</b>
	Timesnet	0.765	0.909	0.831	0.635	0.869	<b>0.734</b>	0.819	0.983	<b>0.894</b>	0.946	0.766	<b>0.847</b>	0.765	0.976	0.858
	$d_{fp}$	1.0	0.885	<b>0.939</b>	1.0	0.894	<b>0.944</b>	1.0	0.892	<b>0.943</b>	1.0	0.955	<b>0.977</b>	1.0	0.849	<b>0.918</b>
	$d_l$	1.0	0.139	0.244	1.0	0.104	0.189	1.0	0.014	0.027	1.0	0.203	0.338	1.0	0.029	0.056
	$d_{disp}$	0.914	1.0	0.955	0.859	1.0	0.924	0.775	1.0	0.874	0.91	1.0	0.953	0.909	1.0	0.952
	$d_{aggr}$	0.961	1.0	<b>0.98</b>	0.98	1.0	<b>0.99</b>	0.962	1.0	<b>0.981</b>	0.99	1.0	<b>0.995</b>	0.948	1.0	<b>0.973</b>
	$d_{cont}$	0.948	1.0	0.973	0.978	1.0	0.989	0.957	1.0	0.978	0.99	1.0	<b>0.995</b>	0.905	1.0	0.95
OIPR	Autoformer	0.196	0.784	0.314	0.209	0.578	0.307	0.955	0.68	0.795	0.828	0.58	0.682	0.997	0.437	0.607
	DLinear	0.458	0.551	<b>0.5</b>	0.271	0.503	<b>0.352</b>	0.883	0.897	<b>0.89</b>	0.84	0.786	<b>0.812</b>	0.981	0.901	<b>0.939</b>
	Timesnet	0.235	0.74	0.357	0.225	0.65	0.334	0.523	0.902	0.662	0.787	0.797	0.792	0.193	0.893	0.317
	$d_{fp}$	1.0	0.424	<b>0.595</b>	0.991	0.418	<b>0.588</b>	0.988	0.359	<b>0.527</b>	0.993	0.91	<b>0.95</b>	0.99	0.388	0.557
	$d_l$	1.0	0.365	0.535	1.0	0.31	0.473	1.0	0.251	0.401	0.95	0.26	0.408	1.0	0.437	<b>0.608</b>
	$d_{disp}$	0.217	0.897	0.349	0.198	0.872	0.322	0.406	0.904	0.56	0.687	0.981	0.808	0.172	0.908	0.29
	$d_{aggr}$	0.811	0.984	<b>0.889</b>	0.821	0.994	<b>0.899</b>	0.913	0.99	<b>0.95</b>	0.83	0.998	<b>0.907</b>	0.854	0.986	<b>0.916</b>
	$d_{cont}$	0.811	0.984	<b>0.889</b>	0.821	0.994	<b>0.899</b>	0.913	0.99	<b>0.95</b>	0.809	0.998	0.894	0.854	0.986	<b>0.916</b>

TABLE VI  
ADDITIONAL STATISTICS FOR THE REAL-WORLD DATASETS.

Statistics		MSL	SMAP	PSM	SMD	SWaT
$N$		73630	427518	87742	7084	449820
$N_a$		36	67	72	118	35
$\bar{L}_a$		216	817	338	3	1561
$d_l$	$L$	500	3000	5000	4	5000
	$R_e(L)$	0.139	0.104	0.014	0.203	0.029
	$R_p(L)$	0.529	0.455	0.365	0.572	0.657
$d_{disp}$	$R_N$	0.946	1.0	0.694	0.345	0.972
$d_{aggr}$	$R_N$	0.108	0.059	0.083	0.017	0.25
$d_{cont}$	$R_N$	0.108	0.059	0.083	0.017	0.25

ground truth events and is an important factor to consider when configuring custom parameters for *TaPR* and *OIPR*.  $N_a$  indicates the total number of anomaly events, while  $L$  refers to the threshold for defining long anomaly events in  $d_l$ . The value  $R_e(L)$  indicates the ratio of long anomaly events out of total anomaly events, and  $R_p(L)$  signifies the ratio of points contained within long anomaly events out of total anomaly points. These statistics provide valuable insights that enhance the understanding of the aforementioned experimental results. For instance, the statistics related to  $d_l$  are employed to support the validation of the conclusions regarding the long anomaly effect observed in the second group of experiments.

## VI. DISCUSSION

In this work, the proposed *OIPR* is characterized as an “area-based” TAD evaluation method. To investigate its correlations and distinctions from existing point-based and event-based methods, we introduce two specific custom configurations of *OIPR*, which can be interpreted as point-based and event-based methods, respectively.

**Zero observation phase.** In this configuration, we assign a value 0 to the parameter  $l_{obs}$  in Algorithm 1, indicating that there is no observation phase associated with the anomaly points. As a result, the operator interest in each anomaly point does not extend to the subsequent time point. It is evident that, in such a scenario, the operator interest curve of the ground truth and that of the detection results can be calculated as:

$$\mathbf{I} = \mathbf{y}, \hat{\mathbf{I}} = \hat{\mathbf{y}}. \quad (10)$$

Hence, *OIPR* degenerates into a point-based method, which is essentially equivalent to the classical *PW* method.

**Strict occurrence detection evaluator.** By setting both  $l_{dis}$  and  $b_{dur}$  to 0, while configuring  $l_{obs}$  to 1 in Algorithm 1, *OIPR* can be transformed into a distinctive event-based method: In this transformed method, a predicted anomaly event is classified as a TP event only when its initial point coincides with the initial point of a ground truth event. Conversely, any ground truth event whose initial point does not align with that of a predicted event is classified as an FN event, while any predicted event whose initial point does not correspond to that of a ground truth event is categorized as an FP event. Although this evaluation method may appear excessively stringent, it

effectively demonstrates that *OIPR* can be transformed into an event-based method through specific parameter configurations.

Through the specific configurations discussed above, it can be observed that *OIPR* lies between the point-based and event-based methods. It employs the observation phase to mitigate the long anomaly effect and to merge potential fragmented events. Additionally, the use of area in calculating the evaluation metrics enables *OIPR* to effectively bridge the gap between point-based and event-based perspectives, thereby enhancing its versatility and applicability.

## VII. CONCLUSIONS

Due to the important role of TAD in data analysis, numerous studies have been carried out to improve the performance of anomaly detectors, aiming to effectively identify anomalous behaviors and potential system faults. In the process of evaluating and comparing various anomaly detectors, we recognize that the selection of evaluation method is a significant factor in promoting the improvement of algorithms for TAD. An appropriate evaluation method not only aids operators in selecting the most effective detector but also prevents researchers from being misled into attaining suboptimal optimization results due to inadequate evaluation methods.

In this work, we conducted a comprehensive comparison of existing evaluation methods and introduced a special scenario dataset. Through experiments on both the special scenario dataset and real-world datasets, we demonstrate the characteristics and limitations of existing evaluation methods. Specifically, we examined the performance of point-based and event-based evaluation methods in addressing various challenges, including the long anomaly effect and the fragmentation effect, which have the potential to lead operators astray in certain situations. Drawing inspiration from the interest of operators in monitoring KPIs and the associated detectors during operational process, we have developed a novel set of TAD evaluation metrics named *OIPR*. Through a series of experiments, we have demonstrated that *OIPR* exhibits fewer limitations and is adaptable to a diverse range of application scenarios. Furthermore, we have discussed the distinctions between *OIPR* with existing point-based and event-based evaluation methods. By customizing its configuration, *OIPR* enables the seamless switching between point-based and event-based evaluation methods, thereby empowering users to achieve a balance between these two distinct perspectives.

## REFERENCES

- [1] Y. Li, X. Peng, J. Zhang, Z. Li, and M. Wen, “DCT-GAN: dilated convolutional transformer-based GAN for time series anomaly detection,” *IEEE Trans. Knowl. Data Eng.*, vol. 35, no. 4, pp. 3632–3644, Apr. 2023.
- [2] J. Xu, H. Wu, J. Wang, and M. Long, “Anomaly transformer: Time series anomaly detection with association discrepancy,” in *The Tenth International Conference on Learning Representations, ICLR 2022*. Virtual Event: OpenReview.net, Apr. 2022, pp. 1–20.
- [3] Y. Su, Y. Zhao, C. Niu, R. Liu, W. Sun, and D. Pei, “Robust anomaly detection for multivariate time series through stochastic recurrent neural network,” in *Proceedings of the 25th ACM SIGKDD International Conference on Knowledge Discovery & Data Mining, KDD 2019*. Anchorage, AK: ACM, Aug. 2019, pp. 2828–2837.

- [4] S. Liu, B. Zhou, Q. Ding, B. Hooi, Z. Zhang, H. Shen, and X. Cheng, "Time series anomaly detection with adversarial reconstruction networks," *IEEE Trans. Knowl. Data Eng.*, vol. 35, no. 4, pp. 4293–4306, Apr. 2023.
- [5] L. Qi, Y. Yang, X. Zhou, W. Rafique, and J. Ma, "Fast anomaly identification based on multiaspect data streams for intelligent intrusion detection toward secure industry 4.0," *IEEE Trans. Ind. Informatics*, vol. 18, no. 9, pp. 6503–6511, Dec. 2022.
- [6] D. Velásquez, E. Pérez, X. Oregui, A. Artetxe, J. Manteca, J. E. Mansilla, M. Toro, M. Maiza, and B. Sierra, "A hybrid machine-learning ensemble for anomaly detection in real-time industry 4.0 systems," *IEEE Access*, vol. 10, pp. 72 024–72 036, Jul. 2022.
- [7] L. Dai, W. Chen, Y. Liu, A. Argyriou, C. Liu, T. Lin, P. Wang, Z. Xu, and B. Chen, "Switching gaussian mixture variational RNN for anomaly detection of diverse CDN websites," in *IEEE INFOCOM 2022 - IEEE Conference on Computer Communications*. London, United Kingdom: IEEE, 2022.
- [8] D. Tang, S. Wang, B. Liu, W. Jin, and J. Zhang, "GASF-IPP: detection and mitigation of Idos attack in SDN," *IEEE Trans. Serv. Comput.*, vol. 16, no. 5, pp. 3373–3384, Apr. 2023.
- [9] X. Li, K. Xie, X. Wang, G. Xie, J. Wen, G. Zhang, and Z. Qin, "Online internet anomaly detection with high accuracy: A fast tensor factorization solution," in *2019 IEEE Conference on Computer Communications, INFOCOM 2019*. Paris, France: IEEE, 2019.
- [10] S. Zhang, Z. Zhong, D. Li, Q. Fan, Y. Sun, M. Zhu, Y. Zhang, D. Pei, J. Sun, Y. Liu, H. Yang, and Y. Zou, "Efficient KPI anomaly detection through transfer learning for large-scale web services," *IEEE J. Sel. Areas Commun.*, vol. 40, no. 8, pp. 2440–2455, Aug. 2022.
- [11] G. Sivapalan, K. K. Nundy, A. P. James, B. Cardiff, and D. John, "Interpretable rule mining for real-time ECG anomaly detection in iot edge sensors," *IEEE Internet Things J.*, vol. 10, no. 15, pp. 13 095–13 108, Mar. 2023.
- [12] T. P. Q. Nguyen, P. N. K. Phuc, Y. C., H. Sutrisno, B. Luong, T. H. A. Le, and T. T. Nguyen, "Time-series anomaly detection using dynamic programming based longest common subsequence on sensor data," *Expert Syst. Appl.*, vol. 213, no. Part, p. 118902, Mar. 2023.
- [13] L. Fang, Y. Li, Z. Liu, C. Yin, M. Li, and Z. Cao, "A practical model based on anomaly detection for protecting medical iot control services against external attacks," *IEEE Trans. Ind. Informatics*, vol. 17, no. 6, pp. 4260–4269, Jul. 2021.
- [14] Y. Zhang, Y. Chen, J. Wang, and Z. Pan, "Unsupervised deep anomaly detection for multi-sensor time-series signals," *IEEE Trans. Knowl. Data Eng.*, vol. 35, no. 2, pp. 2118–2132, Feb. 2023.
- [15] M. Kravchik and A. Shabtai, "Detecting cyber attacks in industrial control systems using convolutional neural networks," in *Proceedings of the 2018 Workshop on Cyber-Physical Systems Security and Privacy, CPS-SPC@CCS 2018*. Toronto, Canada: ACM, 2018.
- [16] D. Li, D. Chen, B. Jin, L. Shi, J. Goh, and S. Ng, "MAD-GAN: multivariate anomaly detection for time series data with generative adversarial networks," in *Artificial Neural Networks and Machine Learning - ICANN 2019: Text and Time Series - 28th International Conference on Artificial Neural Networks*. Munich, Germany: Springer, 2019.
- [17] S. Ahmad, A. Lavin, S. Purdy, and Z. Agha, "Unsupervised real-time anomaly detection for streaming data," *Neurocomputing*, vol. 262, pp. 134–147, Jul. 2017.
- [18] S. Kim, K. Choi, H. Choi, B. Lee, and S. Yoon, "Towards a rigorous evaluation of time-series anomaly detection," in *Thirty-Sixth AAAI Conference on Artificial Intelligence, AAAI 2022*. California, USA: AAAI Press, 2022, pp. 7194–7201.
- [19] N. Tatbul, T. J. Lee, S. Zdonik, M. Alam, and J. Gottschlich, "Precision and recall for time series," in *Advances in Neural Information Processing Systems 31: Annual Conference on Neural Information Processing Systems 2018, NeurIPS 2018*, Montréal, Canada, 2018, pp. 1924–1934.
- [20] J. Paparrizos, P. Boniol, T. Palpanas, R. Tsay, A. J. Elmore, and M. J. Franklin, "Volume under the surface: A new accuracy evaluation measure for time-series anomaly detection," *Proc. VLDB Endow.*, vol. 15, no. 11, pp. 2774–2787, Sep.
- [21] Y. Xu, W. Chen, N. Zhao, Z. Li, J. Bu, Z. Li, Y. Liu, Y. Zhao, D. Pei, Y. Feng, J. Chen, Z. Wang, and H. Qiao, "Unsupervised anomaly detection via variational auto-encoder for seasonal kpis in web applications," in *Proceedings of the 2018 World Wide Web Conference on World Wide Web, WWW 2018*. Lyon, France: ACM, Apr. 2018.
- [22] W. Hwang, J. Yun, J. Kim, and H. Kim, "Time-series aware precision and recall for anomaly detection: Considering variety of detection result and addressing ambiguous labeling," in *Proceedings of the 28th ACM International Conference on Information and Knowledge Management, CIKM 2019*. Beijing, China: ACM, 2019, pp. 2241–2244.
- [23] W. G. Gadallah, H. M. Ibrahim, and N. M. Omar, "A deep learning technique to detect distributed denial of service attacks in software-defined networks," *Comput. Secur.*, vol. 137, p. 103588, Feb. 2024.
- [24] J. Ahmed and R. C. Green, "Cost aware LSTM model for predicting hard disk drive failures based on extremely imbalanced S.M.A.R.T. sensors data," *Eng. Appl. Artif. Intell.*, vol. 127, no. Part B, p. 107339, Jan. 2024.
- [25] N. Zhao, J. Chen, Z. Yu, H. Wang, J. Li, B. Qiu, H. Xu, W. Zhang, K. Sui, and D. Pei, "Identifying bad software changes via multimodal anomaly detection for online service systems," in *ESEC/FSE '21: 29th ACM Joint European Software Engineering Conference and Symposium on the Foundations of Software Engineering*. Athens, Greece: ACM, Aug. 2021, pp. 527–539.
- [26] A. Huet, J. M. Navarro, and D. Rossi, "Local evaluation of time series anomaly detection algorithms," in *The 28th ACM SIGKDD Conference on Knowledge Discovery and Data Mining, KDD 2022*. Washington, DC: ACM, Aug. 2022, pp. 635–645.
- [27] Y. Lu, R. Wu, A. Mueen, M. A. Zuluaga, and E. J. Keogh, "Matrix profile XXIV: scaling time series anomaly detection to trillions of datapoints and ultra-fast arriving data streams," in *The 28th ACM SIGKDD Conference on Knowledge Discovery and Data Mining, KDD 2022*. Washington, DC: ACM, Aug. 2022, pp. 1173–1182.
- [28] J. Á. Cid-Fuentes, C. Szabo, and K. Falkner, "Adaptive performance anomaly detection in distributed systems using online svms," *IEEE Trans. Dependable Secur. Comput.*, vol. 17, no. 5, pp. 928–941, Sep. 2020.
- [29] A. Deng and B. Hooi, "Graph neural network-based anomaly detection in multivariate time series," in *Thirty-Fifth AAAI Conference on Artificial Intelligence, AAAI 2021*. Virtual Event: AAAI Press, Feb. 2021.
- [30] J. A. Ward, P. Lukowicz, and H. Gellersen, "Performance metrics for activity recognition," *ACM Trans. Intell. Syst. Technol.*, vol. 2, no. 1, pp. 6:1–6:23, Jan. 2011.
- [31] S. Sørbo and M. Ruocco, "Navigating the metric maze: a taxonomy of evaluation metrics for anomaly detection in time series," *Data Min. Knowl. Discov.*, vol. 38, no. 3, pp. 1027–1068, May 2024.
- [32] K. Hundman, V. Constantinou, C. Laporte, I. Colwell, and T. Söderström, "Detecting spacecraft anomalies using lstms and non-parametric dynamic thresholding," in *Proceedings of the 24th ACM SIGKDD International Conference on Knowledge Discovery & Data Mining, KDD 2018*. London, UK: ACM, 2018, pp. 387–395.
- [33] A. Abdulaal, Z. Liu, and T. Lancewicki, "Practical approach to asynchronous multivariate time series anomaly detection and localization," in *KDD '21: The 27th ACM SIGKDD Conference on Knowledge Discovery and Data Mining*. Singapore: ACM, 2021, pp. 2485–2494.
- [34] A. P. Mathur and N. O. Tippenhauer, "Swat: a water treatment testbed for research and training on ICS security," in *2016 International Workshop on Cyber-physical Systems for Smart Water Networks, CySWater@CPSWeek 2016*. Vienna, Austria: IEEE Computer Society, 2016, pp. 31–36.
- [35] H. Wu, J. Xu, J. Wang, and M. Long, "Autoformer: Decomposition transformers with auto-correlation for long-term series forecasting," in *Advances in Neural Information Processing Systems 34: Annual Conference on Neural Information Processing Systems 2021, NeurIPS 2021*, Virtual Event, Dec. 2021, pp. 22 419–22 430.
- [36] A. Zeng, M. Chen, L. Zhang, and Q. Xu, "Are transformers effective for time series forecasting?" in *Thirty-Seventh AAAI Conference on Artificial Intelligence, AAAI 2023*. Washington, DC: AAAI Press, 2023, pp. 11 121–11 128.
- [37] H. Wu, T. Hu, Y. Liu, H. Zhou, J. Wang, and M. Long, "Timesnet: Temporal 2d-variation modeling for general time series analysis," in *The Eleventh International Conference on Learning Representations, ICLR 2023*. Kigali, Rwanda: OpenReview.net, 2023.



**Yuhan Jing** obtained her master's degree from Beijing University of Posts and Telecommunications, China, in 2020. She is currently a doctoral candidate at the State Key Laboratory of Networking and Switching Technology at the Beijing University of Posts and Telecommunications. Her research interests include AIOps, Time-series Analysis, Anomaly Detection, and Fault Localization.



**Jingyu Wang** obtained his PhD degree from Beijing University of Posts and Telecommunications in 2008. He is currently a professor of the State Key Laboratory of Networking and Switching Technology at Beijing University of Posts and Telecommunications. He is a senior member of the China Communication Society and was selected for the Beijing Young Talents Program. He has published more than 100 papers in international journals or conferences, including IEEE CMag, TSC, TMM, CVPR, ACL, ICDE, AAAI, and so on. His research

interests span broad aspects of Intelligent Networks, Edge/Cloud Computing, Machine Learning, AIOps, IoV/IoT, SDN/NFV, Knowledge-Defined Network, and Intent-Based Networking.



**Zirui Zhuang** received the B.S. and Ph.D. degrees from the Beijing University of Posts and Telecommunications in 2015 and 2020, respectively. He is currently an associate researcher with the State Key Laboratory of Networking and Switching Technology, Beijing University of Posts and Telecommunications. In 2019, he visited the Department of Electrical and Computer Engineering, University of Houston. His research interests involve network routing and management for next-generation network infrastructures, using machine learning and

artificial intelligence techniques, including deep learning, reinforcement learning, graph representation, multi-agent systems, and Lyapunov-based optimization.



**Lei Zhang** received her master degree from Nanjing University of Posts and Telecommunications in 2004. She is the technical expert of department of Cloud Network Center at China Unicom, and the leader of Digital twin Project. Her research interest covers mobile network, Network Management, AIOps, Digital twin etc.



**Chengsen Wang** obtained his B.D. degree from Beijing University of Posts and Telecommunications in 2022. He is currently a doctoral candidate of State Key Laboratory of Networking and Switching Technology at Beijing University of Posts and Telecommunications. His main research interests include time series analysis, anomaly detection, and multimodal learning.



**Haifeng Sun** obtained his PhD degree from Beijing University of Posts and Telecommunications in 2017. He is currently an associate professor of the State Key Laboratory of Networking and Switching Technology at Beijing University of Posts and Telecommunications. His research interests span broad aspects of AI, NLP, big data analysis, object detection, deep learning, deep reinforcement learning, SDN, and processing.



**Qi Qi** obtained her PhD degree from Beijing University of Posts and Telecommunications in 2010. Now, she is a professor at the State Key Laboratory of Networking and Switching Technology at the Beijing University of Posts and Telecommunications. She has published more than 30 papers in international journals or conferences, and obtained two National Natural Science Foundations of China. Her research interests include edge intelligence, the Internet of Things, multimedia services, deep reinforcement learning, and distributed machine learning.



**Bo He** obtained his PhD degree from Beijing University of Posts and Telecommunications, China, in 2023. He is currently a postdoctoral researcher of the State Key Laboratory of Networking and Switching Technology at the Beijing University of Posts and Telecommunications. From 2021 to 2022, He was a visiting PhD student at the University of Waterloo, Canada. His research interests include 5G/6G networks, multipath networks, collective communication, transmission control, and deep reinforcement learning.



**Jianxin Liao** obtained his PhD degree at the University of Electronics Science and Technology of China in 1996. He is currently the dean of the Network Intelligence Research Center and the full professor of the State Key Laboratory of Networking and Switching Technology at the Beijing University of Posts and Telecommunications. He has published hundreds of research papers and several books. He has won a number of prizes in China for his research achievements, which include the Premier's Award of Distinguished Young Scientists from the National

Natural Science Foundation of China in 2005, and the Specially-invited Professor of the "Yangtze River Scholar Award Program" by the Ministry of Education in 2009. His main research interests include cloud computing, mobile intelligent network, service network intelligence, networking architectures and protocols, and multimedia communication.

## APPENDIX

## INTRODUCTION AND EXPERIMENTAL RESULTS OF THE SPECIAL SCENARIO DATASET

The appendix presents the introduction and experimental results of the special scenario dataset proposed in this work. It comprises nine distinct scenarios, each highlighting one or two evaluator characteristics. Visualizations of all special scenarios are presented in Fig. A1, while the experimental results for different evaluation methods are summarized in Table A1. The detailed descriptions of the special scenarios are as follows:

**Overlap proportion.** The ground truth comprises a single anomaly event spanning 50 points, with predicted anomaly proportions varying across cases  $c1$  to  $c4$ : the first point only, the initial 20%, 52%, and 100% of the points, respectively. Evaluators that yield a higher f1-score for  $c1$  compared to  $PW$  exhibit the characteristic of existence detection reward. Additionally, those able to differentiate  $c2$ ,  $c3$ , and  $c4$  based on f1-scores demonstrate the overlapping proportion awareness.

**Fragmented TPs.** In this scenario, the ground truth consists of a 30-point anomaly event, detected in varying completeness across three cases, each containing an FP point. In  $c1$  to  $c3$ , the ground truth event is detected as one complete event, three fragmented events, and ten fragmented events, respectively. Both  $c2$  and  $c3$  encompass a total of 20 TP points. Evaluators with the fragmented results penalty characteristic assign a lower recall to  $c3$  than  $c2$ , while those exhibiting the fragmentation misleading in precision characteristic yield higher precision scores for  $c2$  and  $c3$  than for  $c1$ .

**Fragmented FPs.** The ground truth consists of a single anomaly event spanning 20 points, which is completely detected. In cases  $c1$  to  $c3$ , varying sets of FP points are introduced into the detection results: 10 dispersed FP points at intervals of 30, 10 aggregated FP points at intervals of 2, and 20 continuous FP points, respectively. Evaluators exhibiting the characteristic of fragments merging assign a significantly lower f1-score to  $c1$  compared to  $c2$  and  $c3$ .

**Temporal shifting.** In this scenario, the ground truth encompasses three anomaly events, each consisting of two anomaly points. In  $c1$ , a virtual early detector identifies anomalies two points prior to each ground truth event. In contrast, in  $c2$ , a virtual delayed detector with a delay of two points is employed. Evaluators that address ambiguous labels yield f1-scores higher than 0 in both cases.

**TP positions.** The ground truth comprises a single anomaly event spanning 30 points. In cases  $c1$  to  $c3$ , the anomaly event is detected at the first, 15th, and last points, respectively. Evaluators with the characteristic of early detection reward assign the highest f1-score to  $c1$ , followed by  $c2$  and  $c3$ .

**Long anomaly effect.** The ground truth consists of a long anomaly spanning 10 points and six short anomalies, each comprises one point. In cases  $c1$  to  $c3$ , the detection results encompass the long anomaly, the six short anomalies, and the long anomaly accompanied by three FP points, respectively. Evaluators with the characteristic of long anomaly misleading exhibit a much higher f1-score for  $c1$  compared to  $c2$ , while the f1-score for  $c3$  is slightly lower than that of  $c1$ .

**Sparse anomalies.** The ground truth comprises two widely spaced anomaly points, of which one is correctly detected

while the other is missed. In contrast to  $c1$ ,  $c2$  includes an additional FP point. The evaluation method of  $AM$  mistakenly treats this FP point as beneficial for the f1-score due to the mapping of absolute distance to relative recall distance. Notably, this characteristic of sparse anomaly misleading is not observed in other evaluators.

**Constant detectors.** The ground truth consists of four anomaly events with lengths of 10, 20, 30, and 40, respectively. In this scenario, two ineffective constant detectors are evaluated: the all\_0 detector ( $c1$ ), which outputs 0 at all time points, and the all\_1 detector ( $c2$ ), which outputs 1 consistently. Despite an f1-score of 0.672 indicating the characteristic of overestimation for the all\_1 detector in the  $AM$  method, this systematic overestimation is not considered to affect the performance ranking of  $AM$  across different detectors. The authors of  $AM$  have stated that its baseline f1-score is 0.5, reflecting the expected value of the random detector, and detectors failing to significantly surpass this baseline are deemed ineffective.  $TaPR$  also shows the characteristic of overestimation for the all\_1 detector with an f1-score of 0.713, which is linked to its custom configuration. Users can mitigate this overestimation by lowering the detection score weight in  $TaPR$  (minimum 0), but this adjustment sacrifice the beneficial characteristic of existence detection reward, highlighting an inherent trade-off between these two characteristics in  $TaPR$ .

**Random detector.** The random detector generates anomalies with a probability of 0.02 at each timestamp over a time-series of 1000 points. In  $c1$ , the ground truth comprises 15 anomaly events, each with a duration of 3 points, representing the case of short anomalies. Conversely,  $c2$  contains a single anomaly event spanning 45 points, illustrating the case of a long anomaly. The evaluation outcome of  $PA$  shows significant overestimation for the random detector on  $c2$ , with an average f1-score of 0.534 across 100 experiments. For the evaluation method of  $AM$ , the overestimation for the random detector is a predictable systematic overestimation, akin to that seen in the all\_1 detector case. Additionally,  $OIPR$  exhibits a slight overestimation in  $c1$  due to the dense distribution of the 15 anomalies in the test dataset. With the parameter  $l_{obs}$  set to 20, there is a resultant partial overlap between the observation phases of the short anomalies. It is recommended to adjust  $l_{obs}$  based on the context of the average anomaly length during practical applications, though we did not implement this adjustment to maintain the simplicity of the experiment.

The aforementioned special scenarios reveal critical boundary conditions that influence the evaluation outcomes. In practice, such special scenarios often arise within specific slices of a dataset. Operators typically lack the time to assess the detailed performance for each detector across all dataset slices, leading them to rely on general feedback from evaluation methods to select the best detector. As a result, the pitfalls of the evaluation method may remain difficult to discern. To address this issue, we propose this purpose-designed special scenario dataset, facilitating cost-effective testing of evaluator characteristics. This will enable operators to select the most suitable evaluator while gaining insights into its limitations. For researchers, a well-defined dataset promotes experimentation with more effective evaluation methods.

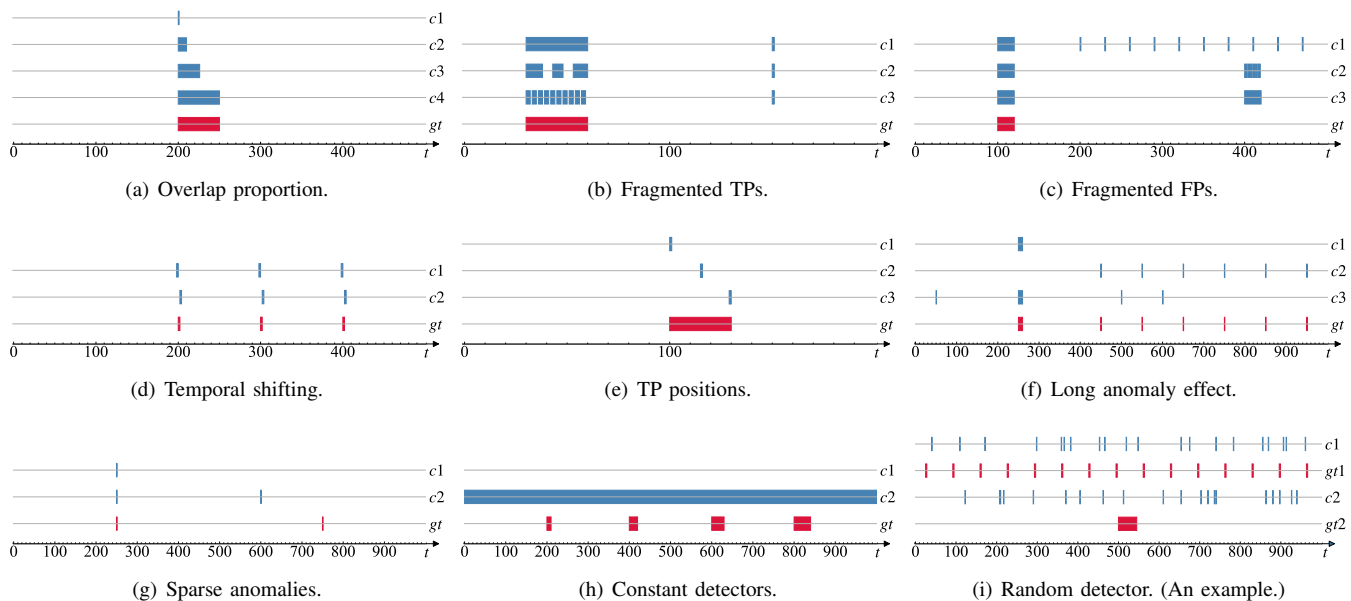


Fig. A1. The visualization of the special scenario dataset. With the exception of the random detector scenario, all cases within a single scenario share the same ground truth (red bar) but yield different detection results (blue bar).

TABLE A1

EXPERIMENTAL RESULTS (P/R/F1) ON THE SPECIAL SCENARIO DATASET. BENEFICIAL CHARACTERISTICS OF EVALUATORS ARE MARKED WITH A STAR (\*) OR A DAGGER (†), WHILE MISLEADING CHARACTERISTICS ARE INDICATED WITH A DIAMOND (◊).

Scenario	Case	PW	PA	PA%K	RP/RR	TaPR	AM	OIPR (Ours)
<b>Overlap proportion</b>	<i>c1</i>	1.0/0.02/0.039	1.0/1.0/1.0*	1.0/0.02/0.039	1.0/0.52/0.684*†	1.0/0.51/0.675*†	1.0/0.904/0.95*†	1.0/0.217/0.356*†
	<i>c2</i>	1.0/0.2/0.333†	1.0/1.0/1.0	1.0/0.2/0.333†	1.0/0.678/0.808*†	1.0/0.6/0.75*†	1.0/0.936/0.967*†	1.0/0.361/0.53*†
	<i>c3</i>	1.0/0.52/0.684†	1.0/1.0/1.0	1.0/1.0/1.0*	1.0/0.882/0.938*†	1.0/0.76/0.864*†	1.0/0.977/0.988*†	1.0/0.617/0.763*†
	<i>c4</i>	1.0/1.0/1.0†	1.0/1.0/1.0	1.0/1.0/1.0†	1.0/1.0/1.0*†	1.0/1.0/1.0*†	1.0/1.0/1.0*†	1.0/1.0/1.0*†
Evaluator characteristics: *existence detection reward, †overlapping proportion awareness.								
<b>Fragmented TPs</b>	<i>c1</i>	0.968/1.0/0.984	0.968/1.0/0.984	0.968/1.0/0.984	0.5/1.0/0.667	0.5/1.0/0.667	0.976/1.0/0.988	0.758/1.0/0.863
	<i>c2</i>	0.952/0.667/0.784	0.968/1.0/0.984	0.968/1.0/0.984	0.75/0.613/0.675*◊	0.75/0.833/0.789◊	0.964/0.996/0.98	0.757/0.993/0.859*
	<i>c3</i>	0.952/0.667/0.784	0.968/1.0/0.984	0.968/1.0/0.984	0.909/0.534/0.673*◊	0.909/0.833/0.87◊	0.964/0.999/0.981	0.754/0.976/0.85*
Evaluator characteristics: *fragmented results penalty, ◊fragmentation misleading in precision.								
<b>Fragmented FPs</b>	<i>c1</i>	0.667/1.0/0.8	0.667/1.0/0.8	0.667/1.0/0.8	0.091/1.0/0.167	0.091/1.0/0.167	0.778/1.0/0.875	0.194/1.0/0.324*
	<i>c2</i>	0.667/1.0/0.8	0.667/1.0/0.8	0.667/1.0/0.8	0.091/1.0/0.167	0.091/1.0/0.167	0.727/1.0/0.842	0.508/1.0/0.674*
	<i>c3</i>	0.5/1.0/0.667	0.5/1.0/0.667	0.5/1.0/0.667	0.5/1.0/0.667	0.5/1.0/0.667	0.59/1.0/0.742	0.5/1.0/0.667*
Evaluator characteristic: *fragments merging.								
<b>Temporal shifting</b>	<i>c1</i>	0.0/0.0/0.0	0.0/0.0/0.0	0.0/0.0/0.0	0.0/0.0/0.0	0.0/0.0/0.0	0.972/0.986/0.979*	0.729/0.729/0.729*
	<i>c2</i>	0.0/0.0/0.0	0.0/0.0/0.0	0.0/0.0/0.0	0.0/0.0/0.0	0.97/0.97/0.97*	0.972/0.986/0.979*	0.729/0.729/0.729*
Evaluator characteristic: *addressing ambiguous labels.								
<b>TP positions</b>	<i>c1</i>	1.0/0.033/0.065	1.0/1.0/1.0	1.0/0.033/0.065	1.0/0.532/0.695*	1.0/0.517/0.681	1.0/0.86/0.925	1.0/0.319/0.483*
	<i>c2</i>	1.0/0.033/0.065	1.0/1.0/1.0	1.0/0.033/0.065	1.0/0.516/0.681*	1.0/0.517/0.681	1.0/0.93/0.964	0.785/0.25/0.38*
	<i>c3</i>	1.0/0.033/0.065	1.0/1.0/1.0	1.0/0.033/0.065	1.0/0.501/0.668*	1.0/0.517/0.681	1.0/0.86/0.925	0.779/0.248/0.376*
Evaluator characteristic: *early detection reward.								
<b>Long anomaly effect</b>	<i>c1</i>	1.0/0.625/0.769◊	1.0/0.625/0.769◊	1.0/0.625/0.769◊	1.0/0.143/0.25	1.0/0.143/0.25	1.0/0.143/0.25	1.0/0.217/0.357
	<i>c2</i>	1.0/0.375/0.545◊	1.0/0.375/0.545◊	1.0/0.375/0.545◊	1.0/0.857/0.923	1.0/0.857/0.923	1.0/0.857/0.923	1.0/0.783/0.878
	<i>c3</i>	0.769/0.625/0.69◊	0.769/0.625/0.69◊	0.769/0.625/0.69◊	0.25/0.143/0.182	0.25/0.143/0.182	0.312/0.192/0.238	0.357/0.217/0.27
Evaluator characteristic: ◊long anomaly misleading.								
<b>Sparse anomalies</b>	<i>c1</i>	1.0/0.5/0.667	1.0/0.5/0.667	1.0/0.5/0.667	1.0/0.5/0.667	1.0/0.5/0.667	1.0/0.5/0.667	1.0/0.5/0.667
	<i>c2</i>	0.5/0.5/0.5	0.5/0.5/0.5	0.5/0.5/0.5	0.5/0.5/0.5	0.5/0.5/0.5	0.7/0.701/0.7◊	0.5/0.5/0.5
Evaluator characteristic: ◊sparse anomaly misleading.								
<b>Constant detector</b>	<i>c1</i>	0.0/0.0/0.0	0.0/0.0/0.0	0.0/0.0/0.0	0.0/0.0/0.0	0.0/0.0/0.0	nan/0.0/nan	0.0/0.0/0.0
	<i>c2</i>	0.1/1.0/0.182	0.1/1.0/0.182	0.1/1.0/0.182	0.025/1.0/0.049	0.554/1.0/0.713◊	0.506/1.0/0.672◊	0.137/0.92/0.238
Evaluator characteristic: ◊overestimation for the all_1 detector.								
<b>Random detector</b>	<i>c1</i>	0.046/0.019/0.027	0.115/0.057/0.076	0.047/0.019/0.027	0.046/0.039/0.042	0.087/0.077/0.08	0.5/0.45/0.47◊	0.179/0.172/0.173
	<i>c2</i>	0.05/0.021/0.029	0.459/0.64/0.534◊	0.05/0.021/0.029	0.05/0.327/0.085	0.054/0.341/0.09	0.497/0.956/0.652◊	0.05/0.194/0.08
Evaluator characteristic: ◊overestimation for the random detector. Ps.: The evaluation of the random detector is based on the average of 100 experiments.								